Available online at www.sciencedirect.com
SCIENCE DIRECT®
Journal of Solid State Chemistry 173 (2003) 216–226
JOURNAL OF SOLID STATE CHEMISTRY
http://elsevier.com/locate/jssc

Magnetic properties related to structure and complete composition analyses of nanocrystalline $La_{1-x}Mn_{1-y}O_3$ powders

G. Dezanneau,[a,*] A. Sin,[b] H. Roussel,[a] M. Audier,[a] and H. Vincent[a]

[a] *Laboratoire des Matériaux et du Génie Physique, BP46, Domaine Universitaire, 38402 Saint Martin d'Hères cedex, France*
[b] *Pirelli Labs S.p.A., viale Sarca 222, Milano 20126, Italy*

Received 9 September 2002; received in revised form 26 November 2002; accepted 11 December 2002

Abstract

Structural and magnetic properties were studied on $La_{1-x}MnO_{3\pm\delta}$ nanocrystalline powders exhibiting different La/Mn ratios. These compounds were prepared using a gel combustion method based on a cation solution soaking by acrylamide polymerization. Structural properties were studied both by transmission electron microscopy and X-ray diffraction (XRD). Complete chemical composition analyses were performed by induced coupled plasma spectroscopy and by iodometric titration. Proportions of parasitic phases in samples, as La_2O_3 or Mn_3O_4, and actual compositions of $La_{1-x}MnO_{3\pm\delta}$ phases were then determined from refinements of XRD data and sample chemical compositions. As a result, perovskite structure is not any more stable for La/Mn < 0.9 as it decomposes into a mixing of $La_{0.9}MnO_3$ and of Mn_3O_4 phases, in agreement with results on thermodynamic equilibrium in the La–Mn–O phase diagram. For La/Mn > 0.9, a high oxygen excess is observed and leads to consider the creation of vacancies on both lanthanum and manganese sites, whose concentrations are evaluated. Magnetic properties agree well with the proposed structures and sample compositions since for La/Mn < 0.9, for which a $La_{0.9}MnO_3$ phase is always found, the Curie temperature remains constant and equal to 295 K (the highest temperature never observed before in such series of compositions), while for La/Mn > 0.9, there is a formation of Mn vacancies giving rise to a lowering of Curie temperature resulting of a frustration of ferromagnetic interactions.
© 2003 Elsevier Science (USA). All rights reserved.

Keywords: Manganite; Defects; Vacancy; Rietveld; Nanopowders

1. Introduction

Manganites perovskites have received considerable interest in recent years after the discovery of a colossal magnetoresistance (CMR) effect in substituted $La_{1-x}A_xMnO_{3+\delta}$ (where A is a divalent cation or a vacancy). A number of works have been devoted to rare earth manganites doped with alkaline-earth elements while less studies have been performed on vacancy-doped manganites $La_{1-x}MnO_{3\pm\delta}$. These last compounds are meanwhile also interesting for applications. Besides, in the case of $La_{1-x}MnO_{3\pm\delta}$ a fundamental problem is still to understand how variations of electrical and magnetic properties are related to both chemical composition and structure variations. Many published experimental results concern compounds with a La/Mn ratio equal to 1 and with different "oxygen excess" contents [1–6]. Let us note that the $LaMnO_{3+\delta}$ formula, quite often used for such compounds, is ambiguous since cation vacancies are generally considered instead of interstitial oxygen anions (i.e. the formula should be written $(LaMn)_{1-x}O_3$). The so-called oxygen excess δ depends on synthesis and thermal treatment conditions, the highest δ values being obtained at low temperature and under highly oxidative atmosphere. It is frequently proposed that δ can reach a value up to 0.15, which corresponds to 5% of La and Mn vacancies. But much higher δ values have also been proposed, e.g. $\delta = 0.26$ [4] or 0.27 [7], equivalent to about 9% of La and Mn vacancies. Concerning the La/Mn vacancy ratio, there are different conclusions: If Van Roosmalen et al. [1] considered that La and Mn vacancies are in equal amount, Toffield and Scott [5], and Mitchell et al. [8] proposed a higher proportion of La vacancies assuming that a La-rich parasitic phase

*Corresponding author. Departament d'electronica, Universitat de Barcelona, Marti i Franquès, 1, Barcelona 08026, Spain. Fax: +34-93-402-11-48.
E-mail address: gdezano@el.ub.es (G. Dezanneau).

0022-4596/03/$ - see front matter © 2003 Elsevier Science (USA). All rights reserved.
doi:10.1016/S0022-4596(03)00027-6

would be formed. The discrepancy between these conclusions holds to the fact that such a La-rich phase would correspond to a non-crystalline lanthanum hydroxide not detected by X-ray diffraction (XRD). Let us mention that from recent molecular dynamic calculations [9], the formation of La vacancies could actually be favored with respect to Mn vacancies due to a lower formation energy.

Several studies on $La_{1-x}MnO_{3\pm\delta}$ compounds (with $0<x<0.3$) have also been published. Results on structural and magnetic properties [10–13] appear however to be very different for compounds of close compositions. When obtained under oxidative atmosphere, these compounds are generally of rhombohedral structure with a $R\bar{3}c$ space group and exhibit ferromagnetic properties. A maximum Curie temperature of 280 K has been reported [13]. From the phase diagram related to $La_{1-x}MnO_{3\pm\delta}$ products and studied by Van Roosmalen et al. [14] it appears that for La/Mn < 0.9 (or $x>0.1$), a phase separation can occur between a lanthanum manganite phase and a manganese oxide phase (Mn_3O_4). Nevertheless, several studies report single $La_{1-x}MnO_{3\pm\delta}$ phases with x values up to 0.2 [11,13]. Besides, as the oxygen content of such compounds has been shown to decrease with La vacancy doping, it has been argued that the charge defect due to lanthanum vacancy is compensated by oxygen vacancy creation rather than by oxidation of Mn^{3+} into Mn^{4+}. Let us note, however, that the temperature of sample preparation should have an influence on competing phenomena as oxygen vacancy formation and $Mn^{3+} \rightarrow Mn^{4+}$ oxidation since oxygen vacancies usually tend to develop with a temperature increase.

In this article, we investigate the effect of defects on structural and magnetic properties in "vacancy-doped manganites". Complete analyses of chemical compositions, microstructures and structures are related to magnetic properties of $La_{1-x}MnO_{3\pm\delta}$ ($-0.02<x<0.34$) crystalline nanopowders, synthesized at low temperature (1100 K) using a gel combustion method. Correlations between complete chemical composition analyses of $La_{1-x}MnO_{3\pm\delta}$ phases and XRD structural refinements are presented. We show that for high vacancy-doping (La/Mn <0.9), the Curie temperature of compounds becomes invariant and equal to 295 K. Such compounds can be deduced to correspond to mixtures of the $La_{0.9}MnO_3$ and Mn_3O_4 phases according to the phase diagram proposed by Van Roosmalen [14]. For lower vacancy-doping level (La/Mn >0.9), XRD structural refinements and results of chemical composition analyses lead to consider vacancies on both La and Mn sites. In this case, the presence of vacancies on manganese sites strongly affects the ferromagnetic properties.

2. Experimental

Lanthanum manganese oxide powders were prepared through a gel combustion process. Acrylamide polymerization was used to form an organic three-dimensional tangled network in a few seconds, where the solution of the respective cations was soaked. In previous works, acrylamide polymerization has been studied and adapted to cover a broad range of high-impact electroceramic oxides [15–17]. As a result of these fundamental studies, the acrylamide gelification process became, for the first time, fast, inexpensive, reproducible, and easy to scale up for obtaining fine powders of complex oxides. Experimental details on the sample preparation have already been presented in Ref. [17]. Let us just recall that after the gel formation the sample is dried in a microwave oven. The resulting xerogels are treated at 1100 K for 5 h under O_2 flow, the heating and the cooling ramp are 120 and 300 K h^{-1}, respectively. The nominal composition of the eight samples fabricated for the present work are indicated in the fifth column of Table 1.

La and Mn contents within each sample were accurately measured by induced coupled plasma

Table 1
Results on samples composition obtained by induced coupled plasma (ICP), titration and Rietveld refinements of X-ray powder diffraction data

Sample	La/Mn[a]	Mn^{4+} (at%)[b]	O/Mn[c]	Overall composition	Manganite analyzed phases[d]
1	1.020(5)	46(2)	3.26(1)	$La_{0.94}Mn_{0.92}O_3$	$La_{0.92}Mn_{0.94}O_3$ (β)
2	0.960(5)	36(2)	3.12(1)	$La_{0.92}Mn_{0.96}O_3$	$La_{0.90}Mn_{0.98}O_3$ (β)
3	0.891(5)	33(2)	3.00(1)	$La_{0.89}MnO_3$	$La_{0.89}MnO_3$ (α)
4	0.865(5)	32(2)	2.95(1)	$La_{0.86}MnO_{2.95}$	$La_{0.89}MnO_3$ (α)
5	0.818(5)	28(2)	2.85(1)	$La_{0.82}MnO_{2.85}$	$La_{0.89}MnO_3$ (α)
6	0.781(5)	25(2)	2.78(1)	$La_{0.78}MnO_{2.78}$	$La_{0.88}MnO_3$ (α)
7	0.735(5)	24(2)	2.75(1)	$La_{0.73}MnO_{2.75}$	$La_{0.89}MnO_3$ (α)
8	0.661(5)	20(2)	2.61(1)	$La_{0.66}MnO_{2.61}$	$La_{0.88}MnO_3$ (α)

[a] Atomic ratio determined by induced coupled plasma (ICP).
[b] Mn^{4+} concentration determined from titration (in at% of the total of Mn atoms).
[c] Oxygen content determined from La/Mn ratio and Mn^{4+} content.
[d] Manganite phase deduced from Rietveld refinements considering (α) model 2 (β) model 3.

spectroscopy on 100 mg sample fractions. Mn^{4+} concentration was determined using a modified iodometric titration technique, which involves separated processes of sample dissolution in concentrated HCl and chlorine absorption by KI solution [18]. As a result, for a typical amount of 50 mg, the statistical error calculated on 3–5 experiments did not exceed 0.01 in δ (oxygen excess) value, which corresponds to $\pm 2\%$ absolute error on Mn^{4+} content.

Sample analyses by XRD were performed on a Siemens D-5000 $\theta/2\theta$ powder diffractometer using a Cu($K\alpha_{1,2}$) wavelength. Data were collected in the Bragg–Brentanno geometry, with a 2θ step of 0.02°, and a counting time of 18 s. All powder XRD spectra were refined using the program FULLPROF [19] which is based on the Rietveld method [20]. Sample microstructure and structure were studied by transmission electron microscopy (TEM) using a JEOL 200CX. In this case, specimens were prepared from ultrasounded suspensions of lanthanum manganite powders in alcohol, which were deposited on copper grids coated with a carbon film. Magnetic measurements were performed on a vibrating sample magnetometer for temperatures varying from 10 to 340 K and under magnetic fields up to 8 T.

3. Results

3.1. Composition and morphology

The variation of Mn^{4+} concentration within samples as a function of their La/Mn ratio presented in Fig. 1 is almost linear, starting from 46% for La/Mn = 1.02 till 20% for La/Mn = 0.66. We also report in this figure the Mn^{4+} content calculated for "ideal" $La_{1-x}MnO_3$ compounds where, on either side of this curve, over- or under-stoichiometry in oxygen might be considered. It is evident that the Mn^{4+} content experimentally measured differs strongly with the one expected for $La_{1-x}MnO_3$ compounds. For low Mn^{4+} concentrations, the reason might be that the charge deficit on La sites is compensated by a formation of oxygen vacancies. However, in this low Mn^{4+} concentration range, the corresponding La/Mn ratio values are related to a region of the phase diagram where a phase separation might occur [14]. Then, for La/Mn < 0.9, the decrease of Mn^{4+} concentration measured by iodometric titration might be due to the formation of a secondary phase namely Mn_3O_4 for which the Mn valence is only 2.66. Let us note that, on account of the highly oxidative atmosphere used for thermal treatments, Mn_3O_4 is more likely formed than oxygen vacancies. In the oxygen excess domain, it seems reasonable to assume that vacancies exist on both La and Mn sites instead of poorly probable interstitial oxygen (see resulting formula in the fifth column of Table 1).

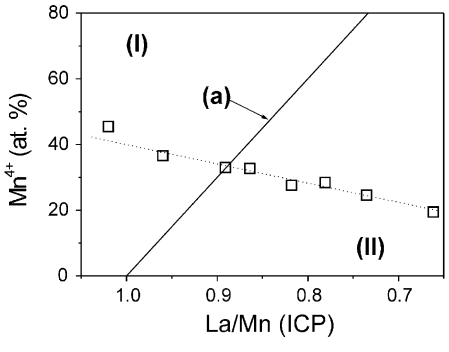

Fig. 1. Mn^{4+} concentration (in at% of the total of Mn cations) determined by iodometric titration versus La/Mn ratios measured by ICP in the samples indicated in Table 1 (square dots). The full line (a) corresponds to the expected variation of $La_{1-x}MnO_3$ phases; domains either over-stoichiometric (I) or under-stoichiometric (II) are defined on either sides of this line.

From TEM observations, we have found that all powder samples exhibit similar foam-like microstructures of small agglomerated polygonal grains of 10–50 nm in size. A bright-field image of such foam-like microstructure is shown in Fig. 2a, corresponding to the sample no. 8 (Table 1). The gelification process (i.e. cationic solution concentration, amount polymerization reagents) and thermal treatment which can determine definitively the morphology of the nanopowders [16] were identical for all samples. Therefore, keeping all the synthesis parameters the same for all samples we obtain similar microstructures. For all samples, grains constituting walls in between bubbles of the foam-like microstructure were found to be of tabular shape. Some of them exhibit a preferential ⟨100⟩ crystallographic direction along their small dimension; for instance, three grains with a common ⟨100⟩ zone axis can be observed in the high-resolution image shown in Fig. 3b and corresponding to the bottom part of the micrograph of Fig. 3a. If similar microstructures were observed for all samples, grain structures appeared however to evolve significantly with the composition; indeed, for sample no. 1, with the lowest La-vacancy concentration, the grains appear to be perfect single crystals (Fig. 3a and b), while for sample no. 8 with the highest La vacancy concentration, defects inside the grains give rise to important contrast variations (Fig. 3c). These contrast variations were associated to the presence of parasitic phases and antiphase boundaries, as identified from selected area electron diffraction pattern (SAED) and from Fourier transformation analyses of high-resolution images. For instance, the SAED image presented in Fig. 2b corresponding to sample no. 8 shows both cubic (or pseudo-cubic) lanthanum manganite perovskite and tetragonal Mn_3O_4 phases. An example of

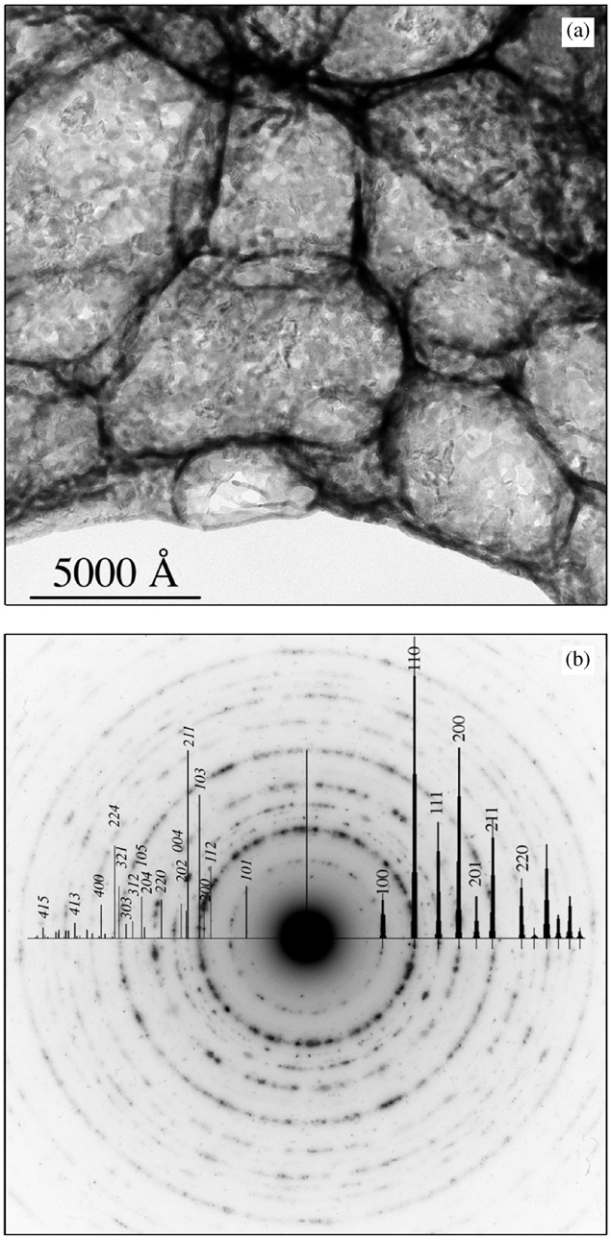

Fig. 2. TEM bright-field image showing the foam-like microstructure observed on the sample no. 8 ($La_{0.66}MnO_{2.61}$ in Table 1) and corresponding electron diffraction pattern with a selected area of 350 nm in diameter, where simulated pattern and indexation of a cubic (or pseudo-cubic) lanthanum manganite perovskite (right side) and tetragonal Mn_3O_4 (left side) phases are presented.

high-resolution result is also shown for the same sample in Fig. 3d. A period of 4.92 Å for lattice fringes corresponding to the {101} plane spacing of the Mn_3O_4 tetragonal structure ($a=5.765$ Å, $c=9.442$ Å, space group $I4_1/amd$) was deduced by Fourier transformation with respect to (100) and (110) reflections of the cubic or pseudo cubic lanthanum manganite phase ($a=3.84$ Å). Some defects were identified to be antiphase boundaries. From high-resolution imaging along a [001] zone axis, they appear to be characteristic of two vectors components 1/2 [100] and 1/2 [010] (Fig. 3e). Thus, assuming that the resulting vector 1/2 [110] might be a characteristic of this antiphase boundary, it appears from a drawing of the perovskite structure that the antiphase boundary would be defined by edge links between oxygen octahedra (Fig. 3f). In this case, it can easily be deduced that such an antiphase boundary is equivalent to a sandwich structure of $a/2$ thickness and MnO_2 composition within the perovskite lattice. Therefore, the overall composition of samples can depend on the amount of these antiphase boundaries according to a formula of the type $LaMn_{1+1/n}O_{3+2/n}$ in the case of one MnO_2 layer of $a/2$ thickness for n layers of $LaMnO_3$ also of $a/2$ thickness. Such defects, which are only observed for highly La-deficient samples, allow the perovskite structure to accommodate La-deficiency like Mn_3O_4 formation does. Antiphase boundaries have also been observed in Mn-rich manganite thin films by Gorbenko et al. [21], who interpreted them as semi-coherent MnO_x inclusions. Let us note that with antiphase boundaries within the manganite phase, the average coherent grain size of manganite phase as analyzed by XRD, must be smaller than the one observed by TEM.

3.2. X-ray diffraction study

Pure manganite phase or a mixing of manganite and Mn_3O_4 phases were identified by powder XRD (Fig. 4). A presence of Mn_3O_4 is apparent for the four higher doping values, but even for long time X-ray acquisitions it was not revealed for the lower ones. From reflections observed in a limited 2θ-range [27°–37.5°] (inset of Fig. 4) the amount of Mn_3O_4 phase appears to increase with a decrease of the La/Mn ratio from sample no. 5 up to a maximum for the sample no. 8 (i.e. $La_{0.66}MnO_{2.61}$). Indexing of the manganite perovskite phase can be realized for all compositions in a rhombohedral system of $R\bar{3}c$ space group using hexagonal axes as shown in Fig. 4. In this hexagonal setting there are 6 formula per unit cell and the atomic site positions are: La (0,0,0.25) in 6 a, Mn (0,0,0) in 6 b and O (x,0,0.25) in 18 e with $x\sim0.45$ [22,23]. Starting from these crystallographic data, Rietveld refinements were performed considering successively three models for atomic occupancies on La, Mn and O sites:

(i) Model 1. The occupancies of all atomic sites were firstly fixed at values corresponding to composition measurements (ICP and titration). Let us mention that such a model does not allow to consider the presence of parasitic phases.
(ii) Model 2. Mn and O sites were considered as fully occupied while the La site occupancy was refined. In this case it was also possible to estimate a proportion of Mn_3O_4 phase within the samples.

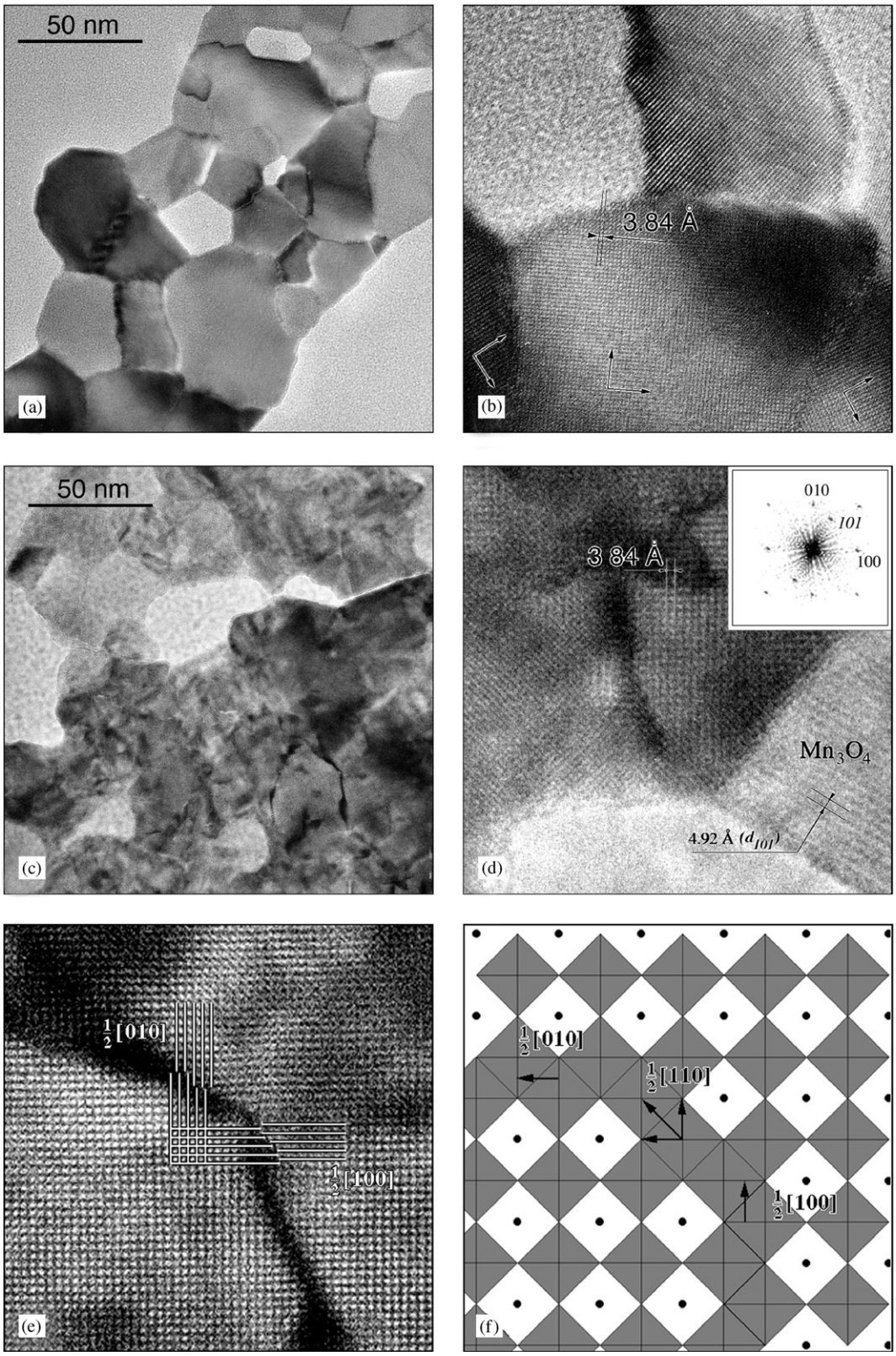

Fig. 3. (a) TEM bright-field and (b) high-resolution images of sample no. 1 ($La_{0.94}Mn_{0.92}O_3$) showing that grains are of tabular shape, without defect and that some of them exhibit a preferential $\langle 100 \rangle$ crystallographic direction along their small dimension; (c) bright-field and (d,e) high-resolution images of the sample no. 8 ($La_{0.66}MnO_{2.61}$) showing in (c) that grains are with defects (giving rise to important contrast variations); in (d) that a grain is identified to be Mn_3O_4 from a Fourier transformation (in inset) of the image and in (e) a defect corresponding to an antiphase boundary characteristic of two vectors components 1/2 [100] and 1/2 [010]. In (f) a drawing of the perovskite structure indicates that the antiphase boundary would be defined by edge links between oxygen octahedra.

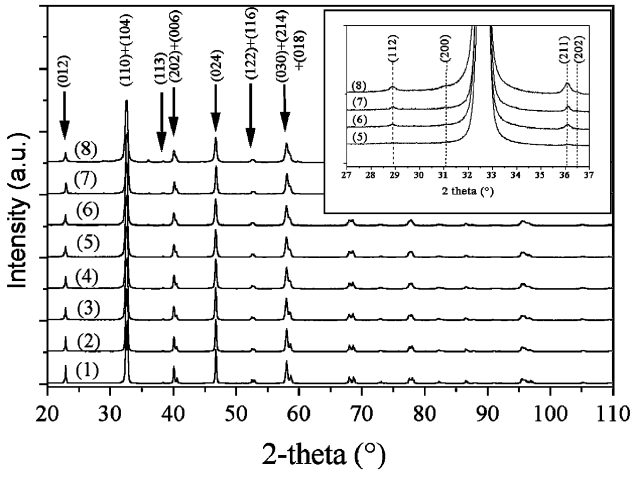

Fig. 4. XRD spectra of sample nos. 1–8, with an indexing in a $R\bar{3}c$ space group (hexagonal representation) of the manganite phases; inset: zoom on spectra of highly vacancy-doped sample nos. 5–8 with indexing of the Mn_3O_4 reflections.

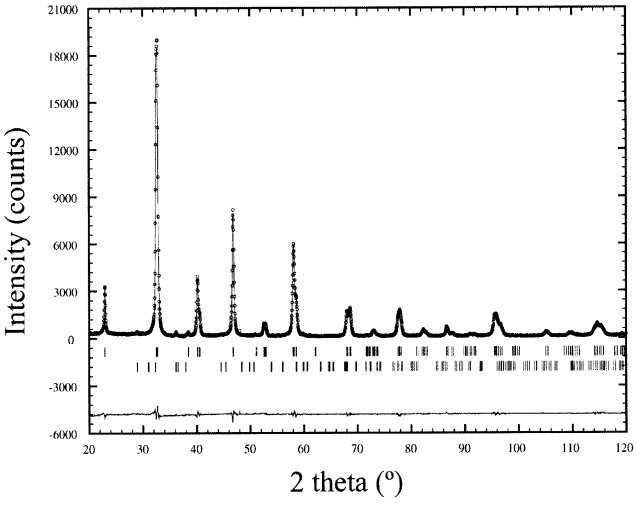

Fig. 5. Experimental (dots), calculated and difference (solid lines) XRD patterns for sample no. 6 using model 2. The vertical bars show the Bragg angle positions, the second line refers to Mn_3O_4 detected as impurity.

(iii) Model 3. On account of results obtained from model 2 and from the chemical composition analyses, the last refinements were carried out in order to determine the amount of vacancies on both La and Mn sites and a proportion of lanthanum oxide phase in sample nos. 1 and 2.

Let us precise that for all samples, isotropic Debye–Waller factors of lanthanum, manganese and oxygen atoms were refined during a last refinement step. Also when present i.e. for sample nos. 6–8 was introduced during refinement the parasitic phase Mn_3O_4. In this latter case, structural information has been taken from Ref. [24]. In Fig. 5, we present an example of refinement results for sample no. 6 (model 2) where both perovskite and Mn_3O_4 phases have been considered.

3.2.1. Models 1 and 2

When fixing La, Mn, and O occupancy factors to those determined from composition measurements (i.e. model 1), several values of reliability factors were found to be quite high (Table 2). This is in particular the case for highly vacancy-doped compounds for which a high amount of vacancies has been considered on lanthanum and oxygen sites. This means that the real formula of the manganite perovskite phase could be significantly different from the one deduced from composition measurements for the whole powder. In the model 2, La/Mn ratios were then varied and the occupancy factor on oxygen sites was fixed to 1 (i.e. on account that compounds were prepared under oxidative atmosphere). As a result, it appears that better agreement factors are obtained. For samples with a La/Mn ratio in between 0.9 and 0.66 (i.e. for sample nos. 3–8), the occupancy factors for La sites become all close to 0.9 (or $x \geqslant 0.1$ in $La_{1-x}MnO_{3\pm\delta}$, sample formula). This means that these powder samples actually consist in a mixture of $La_{0.9}MnO_3$ manganite phase and, at least, a Mn-rich phase since the overall La/Mn ratio in these samples is equal or lower than 0.9. This Mn-rich phase corresponds to Mn_3O_4, identified both by electron and XRD. Therefore, it is possible to calculate a mean Mn valence for samples when considering that (i) both La/Mn and O/Mn ratios in the manganite phase correspond to those obtained from Rietveld refinements and (ii) the rest of Mn (deduced from a balance with ICP data) corresponds to Mn_3O_4. As reported in Fig. 6, the results of such calculations obtained from model 2 exhibit a very good agreement with measured Mn^{4+} content for La/Mn < 0.9.

3.2.2. Model 3

For low doping ($x < 0.1$ or La/Mn > 0.9), occupancy factors on La sites are smaller than those expected from ICP results (Table 2). In such a case, one can assume that a La-rich parasitic phase La_2O_3 was formed. However, for sample nos. 1 and 2, no agreement was found between measured Mn^{4+} content and those calculated from model 2 (Fig. 6). Vacancies on Mn sites should then be assumed. But, as Debye–Waller and occupancy factors are strongly coupled, a direct refinement of all these parameters could not be performed. We have proceeded in three steps, as follows:

(i) Thermal parameters were refined for occupancy factors on La and Mn sites varying between 0.9 and 1 in order to define the most probable Mn site occupancy for a given La site occupancy from a mapping of the corresponding χ^2 values. For

Table 2
Refined cell parameters, atomic positions, occupancies, Debye–Waller factors and agreement factors obtained from three structural models as described in the text

Sample no.	1	2	3	4	5	6	7	8
La/Mn[a]	1.02	0.96	0.891	0.865	0.818	0.781	0.735	0.661
Cell parameters								
a (Å)	5.5078(1)	5.5065(1)	5.5097(1)	5.5087(1)	5.5073(1)	5.5071(2)	5.5098(1)	5.5065(2)
c (Å)	13.3099(3)	13.3284(3)	13.3395(3)	13.3445(4)	13.3463(4)	13.3503(5)	13.3529(4)	13.3547(7)
x[b]	0.456(1)	0.456(1)	0.455(1)	0.458(1)	0.456(1)	0.459(1)	0.454(1)	0.459(1)
Model 1								
R_{wp}	10.9	10.4	11.5	10.5	12.3	21.3	15.7	19.8
R_{Bragg}	3.74	3.61	2.53	2.95	2.81	3.57	4.49	5.28
χ^2	3.64	3.34	2.11	3.42	2.34	4.30	3.67	5.19
B_{La} (Å^2)	1.05(2)	0.92(2)	0.78(2)	0.75(2)	0.58(2)	0.49(2)	0.43(2)	0.23(3)
B_{Mn} (Å^2)	0.32(3)	0.34(3)	0.67(2)	0.88(3)	0.99(2)	1.28(3)	1.66(3)	2.17(4)
B_O (Å^2)	1.82(11)	1.68(10)	1.71(8)	2.05(11)	1.53(9)	1.71(13)	1.98(11)	2.11(15)
Model 2								
R_{wp}	10.7	10.1	11.4	10.3	11.9	10.1	11.5	12.6
R_{Bragg}	2.94	3.02	2.47	2.79	2.42	2.12	1.97	2.27
χ^2	3.50	3.18	2.04	3.22	2.15	2.92	1.98	2.16
B_{La} (Å^2)	0.97(2)	0.86(2)	0.77(2)	0.81(2)	0.70(2)	0.67(2)	0.72(2)	0.66(3)
B_{Mn} (Å^2)	0.60(4)	0.58(4)	0.65(3)	0.64(4)	0.579(3)	0.55(3)	0.51(3)	0.57(3)
B_O (Å^2)	1.15(2)	1.52(11)	1.75(9)	2.07(11)	1.79(9)	1.65(11)	1.49(9)	1.56(10)
La occ.	0.979(2)	0.922(3)	0.891(2)	0.894(3)	0.887(2)	0.882(3)	0.889(2)	0.879(3)
Model 3								
R_{wp}	10.8	10.2						
R_{Bragg}	3.34	3.20						
χ^2	3.53	3.22						
B_{La} (Å^2)	1.00(2)	0.87(2)						
B_{Mn} (Å^2)	0.58(3)	0.59(3)						
B_O (Å^2)	1.92(11)	1.76(10)						
La occ.	0.922	0.902						
Mn occ.	0.937	0.979						

[a] Overall La/Mn ratio determined from ICP.
[b] Refined value of x for oxygen site position (x, 0, 1/4) in 18e.

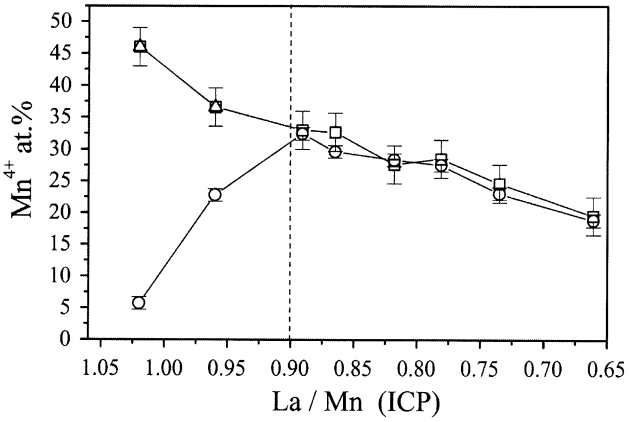

Fig. 6. Comparison of Mn^{4+} content (in at%) versus La/Mn ratios as deduced from chemical composition analyses (open squares) and from Rietveld refinements using both the model 2 (filled circles) and 3 (filled triangles) described in the text.

instance, from such a χ^2 mapping obtained for the sample no. 1 (Fig. 7a), one defines in Fig. 7b that the most probable La/Mn ratios correspond to a very small range of values [0.983–0.99] for a La site occupancy varying from 0.9 to 1.

(ii) Thus, a cation vacancy concentration could be estimated by combining these results to those obtained from chemical composition analyses. From a $La_{1-y}Mn_{1-z}O_3$ chemical formula and assuming a presence of La_2O_3 phase, one can write the following equation:

$$La_{1-x}MnO_{3+\delta} = \frac{1}{1-z}La_{1-y}Mn_{1-z}O_3 + \frac{1}{2}\left(1-x-\frac{1-y}{1-z}\right)La_2O_3,$$

where x is deduced from ICP measurements and δ from titration; y and z correspond to vacancy concentrations on La and Mn sites, respectively. As from results of Rietveld refinements y and z are related between them, it is possible to determine the vacancy concentration on both La and Mn sites. For the sample no. 1, we have found an occupancy of 0.922 on La site and 0.935 on Mn site

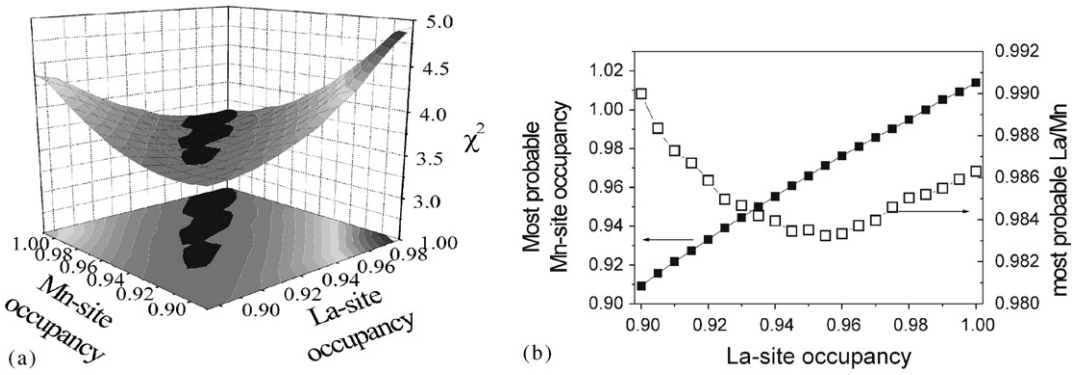

Fig. 7. Map of χ^2 reliability factor as a function of La- and Mn-site occupancy (a) from which the most probable Mn-site occupancy and La/Mn ratio are deduced as a function of La-site occupancy (b).

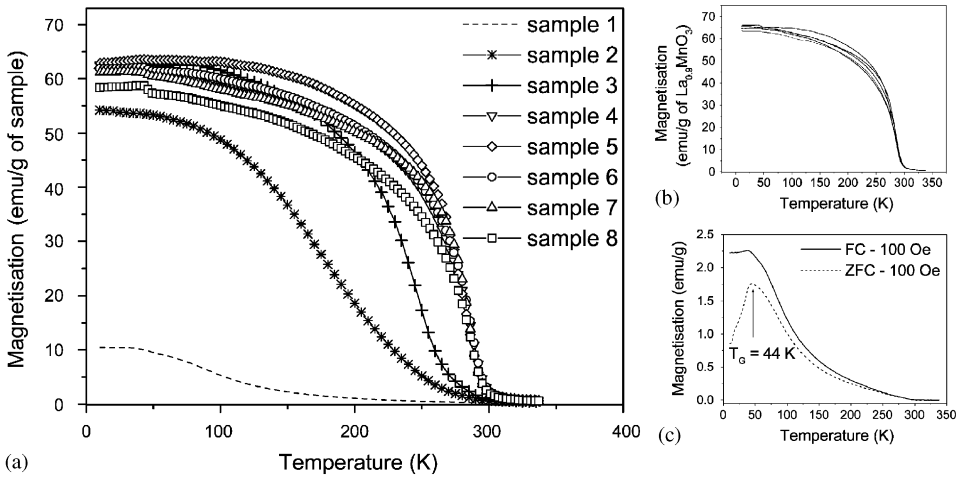

Fig. 8. (a) Magnetization as a function of temperature for sample nos. 1–8, (b) magnetization normalized to the content of manganite phase $La_{0.9}MnO_3$ in sample nos. 4–8, (c) magnetizations under zero-field cooling (ZFC) and field cooling (FC) observed on the sample no. 1 and which are characteristic of spin glass transition.

and, for the sample no. 2, 0.901 and 0.979 for La and Mn site occupancies, respectively.

(iii) Such occupancy factors were then used for new refinements, referred to model 3 in Tables 1 and 2.

Although the agreement factors are a bit higher than those obtained from the model 2 (Table 2), the results of model 3 are now in agreement with composition data (Fig. 6). However, results of model 3 suppose the presence of a La_2O_3 phase, which has not been detected by XRD. The reason of this, as proposed by Tofield and Scott [5], is that lanthanum oxide rapidly converts into lanthanum hydroxide which, being poorly crystalline, evades XRD detection. Several authors [25,26] have indeed confirmed a transformation of La_2O_3 into $La(OH)_3$ in presence of humid air and then into $LaCO_3OH$ through a reaction with atmospheric CO_2. We thus have treated the sample no. 1 at 373 K for 3 weeks under saturated humid air. After such a treatment, we have indeed identified a lanthanum hydroxide carbonate $LaCO_3OH$ phase by XRD. The relative reflection intensities of lanthanum manganite phase being not affected by such a treatment, the model 3 applied to the sample nos. 1 and 2 was also confirmed to be valid.

3.3. Magnetic properties

Magnetizations were measured as a function of temperature in a magnetic field of 0.2 T (Fig. 8a). The sample nos. 4–8 exhibit similar magnetic behaviors and a same Curie temperature of 295 ± 2 K. Let us note that the ferrimagnetic transition at 42 K of Mn_3O_4 is also detected, especially on the sample no. 8 for which the Mn_3O_4 proportion is the largest. From the preceding structural analyses, sample nos. 3–8 were found to be constituted of only two phases, $La_{0.89}MnO_3$ and Mn_3O_4 mixed in different proportions. One can then assume that their magnetization mainly results in a linear

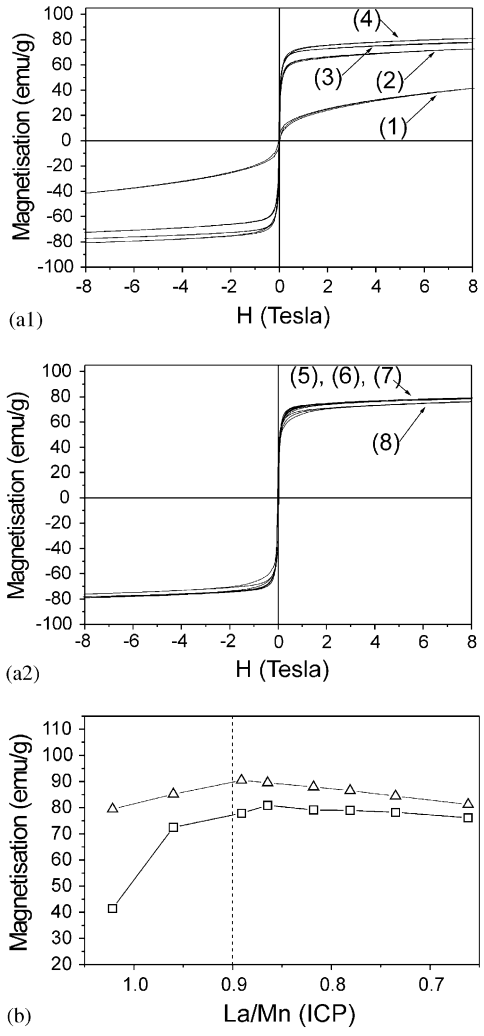

Fig. 9. Hysteresis cycle at 10 K for sample nos. 1–4 (a1) and sample nos. 5–8 (a2), (b) magnetization measured at 10 K under an excitation field of 8 T (open squares) and saturated magnetization calculated from Rietveld models (open triangles) for sample nos. 1–8 (see text).

combination of only two contributions, at least for sample nos. 4–8 which exhibit a same Curie temperature. Thus, from a new plot of the magnetization measured on these samples, but expressed in emu/g of $La_{0.89}MnO_3$ phase as a function of temperature, it appears that the corresponding curves almost superimposed (Fig. 8b). The plot is made for $T > 50$ K in order to exclude the magnetic contribution of Mn_3O_4. However, the curves are not perfectly superimposed probably because of differences in sample microstructures, in particular different average grain sizes as determined from XRD (see Fig. 10a). Although the sample no. 3 was also found to be of composition $La_{0.89}MnO_3$ (Table 1), its Curie temperature of about 270 K is lower than those of sample nos. 4–8. In this case, one has therefore to find out what sample characteristic (not detected from XRD) could be at the origin of this magnetic change. We shall discuss this result after examining the magnetic behavior of the other samples. For La/Mn > 0.9, magnetic transitions become broader with decreasing Curie temperatures for increasing La/Mn ratios. Such magnetic changes for sample nos. 1 and 2 being related to an appearance of vacancies on Mn sites within manganite phases (Table 1); an interpretation could then be that vacancies on manganese sites progressively impede double-exchange ferromagnetic interactions at a long-range scale. This seems to be in accordance with the fact that a spin glass transition was even observed from zero-field cooling (ZFC)—field cooling (FC) measurements on the sample no. 1 (Fig. 8c). Magnetizations as a function of the applied field were also measured on each sample at 10 K up to 8 T (Fig. 9a1 and a2). Departure from magnetic saturation can be estimated quite small for almost all samples, except for the sample no. 1. These magnetizations at 8 T can be compared to calculated values (Fig. 9b) assuming either single-phase systems or mixings of manganite and parasitic phases as determined from Rietveld refinements. In the latter case, a Mn_3O_4 contribution of 42 emu/g to magnetization was considered in calculated values. The discrepancy observed between experimental and calculated values cannot only be the result of unsaturated magnetizations. It is then probably due to the small crystallite size in our samples. Indeed, several studies reporting the influence of grain size on magnetic properties [27,28] show that long-range ferromagnetic order may suffer severe degradation as the particle size decreases, reflected by a general broadening of magnetic transition and a decrease of magnetic susceptibility. Balcells et al. [27] argued for the presence of a non-collinear ferromagnetic surface layer, whose weight increases as crystallite size decreases. They also show that this layer would be magnetically hard after the observation of non-saturated magnetization and high-field magnetoresistance (HFMR) in granular systems. Assuming spherical grains, they propose to calculate the thickness e of this layer according to the following equation:

$$e = \frac{t}{2}\left[1 - \left(\frac{M_s}{M_t}\right)^{1/3}\right],$$

where t is the crystallite or grain size, M_s the measured magnetization at 10 K under an excitation field of 8 T and M_t the theoretical expected magnetization. Average grain sizes (Fig. 10a) in our samples were determined from XRD data applying the Debye–Scherrer law to the reflection (024) at $2\theta = 48°$. From this, calculations of non-collinear layer thickness in samples were performed using the above equation. It appears (Fig. 10b) that such a layer thickness remains nearly constant at a value of about 0.5 nm for La/Mn < 0.9, in rather good agreement with a value of 0.8 nm previously reported by Ballcells

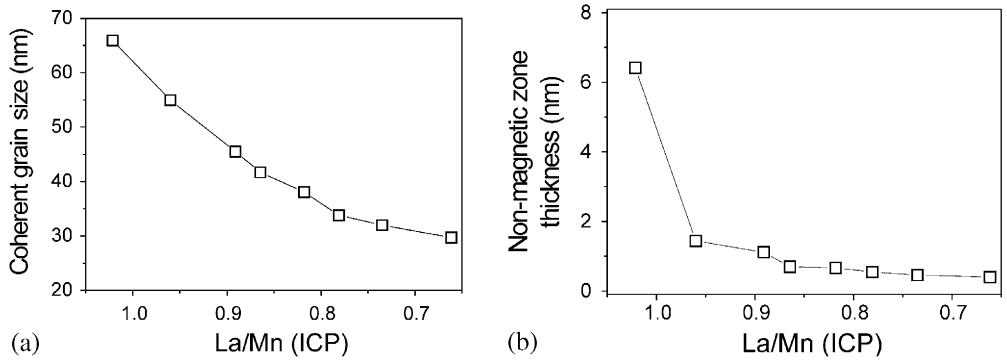

Fig. 10. (a) Variation of the coherent grain size determined from X-ray data on sample nos. 1–8 and (b) variation of the non-magnetic zone thickness versus La/Mn ratio (ICP) determined from a formalism proposed by Balcells et al. [27] (see text).

et al. [27] for a $La_{0.7}Sr_{0.3}MnO_3$ sample containing crystallites of 50 nm in average size. Meanwhile, the important difference observed between measured and calculated magnetization for sample no. 1 cannot only be attributed to a grain size effect. This confirms that vacancies on Mn sites would lead to a high frustration of ferromagnetic interactions.

Coming back to the case of the sample no. 3, it appears on the one hand that its overall composition, although very close to a composition domain giving rise to formation of manganese-deficient manganite phases, does not belong to such a domain. But, on the other hand, one should conclude that its manganite phase might contain a small concentration of vacancies on Mn sites from magnetic measurements. Inaccuracies in both chemical analyses and XRD data refinements might of course be invoked if the observed loss of magnetism does result from a very small concentration of such Mn vacancies.

3.4. Discussion

In summary, for La/Mn < 0.9, Rietveld refinements led us to think that samples consist of a unique manganite phase with a La/Mn ratio close to 0.9 mixed with a Mn_3O_4 phase. This result is consistent with the La_2O_3–Mn_2O_3 phase diagram proposed by Van Roosmalen et al. [14]. Besides, measurements of Mn^{4+} concentrations are in agreement with the hypothesis of such phase equilibrium. Indeed, decreasing values of Mn^{4+} content with x could be attributed to an increasing amount of Mn_3O_4 phase. A constant value of Curie temperature observed in this range of sample compositions also supports that the La-site occupancy factor remains at a constant value of about 0.9. In this range of sample composition, we have also assumed that the Mn and O site occupancies remain both equal to 1. Such an assumption does not appear, a priori, to be in agreement with conclusions of previous works on similar compounds showing that the charge deficit on La sites is compensated by oxygen vacancies [10–13]. In fact, these studies have been performed on compounds synthesized at high temperature, at least 1350 K, for which the charge compensation by oxygen vacancies does likely occur. In our case, considering the low synthesis temperature of samples ($T = 1100$ K) and the oxidative atmosphere used, we can rather suggest that La vacancies are preferentially compensated in the manganite phase by oxidation of Mn^{3+} into Mn^{4+}. This is supported by a high Curie temperature of 295 K, never observed before, which is consistent with a full occupancy on O sites and with a Mn^{4+} concentration close to 33%, corresponding to the proposed $La_{0.89}MnO_3$ composition.

For samples with La/Mn ratios of either 1.02 or 0.96, we have determined that manganite phases contain either 6.5% or 2% of vacancies on Mn sites and 8% or 10% of vacancies on La sites, respectively. The low magnetization values observed at 10 K and under 8 T for these two compounds cannot be explained by only considering the small grain size in samples. It is thus related to the increasing amount of vacancies on Mn sites. The role of such vacancies is likely to hinder Mn-e_g electron hopping that mediates double-exchange ferromagnetic interactions. Super-exchange interactions between nearest Mn cation neighbors could then become dominant. Since local arrangement varies in space because of defects, there must be a strength and sign distribution of exchange interactions. Several interpretations of unsaturated magnetic behaviors on manganese-deficient compounds have been proposed in the literature. For instance, Töpfer et al. [6] mention that according to a trapping mechanism, vacancy-rich domains containing enough Mn^{4+} might be antiferromagnetic within a ferromagnetic matrix, thus leading to magnetic inhomogeneity, which impedes a full magnetization. On the other hand, the observation of a high frustration in a manganese-deficient $La_{0.95}Mn_{0.95}O_3$ compound has been attributed to a cluster-glass behavior. This was supported by results of small angle

neutron scattering experiments [29]. A charge ordering has also been invoked as an explanation of non-saturated magnetic behavior of a $LaMn_{0.9}O_3$ compound [30]. In our case, a concentration of 46% of Mn^{4+} in a highly manganese-deficient $La_{0.92}Mn_{0.94}O_3$ compound could, a priori, be favorable to a charge ordering effect. However, as from recent low-temperature neutron diffraction experiments (not presented here) antiferromagnetic modes were not observed, we think that a cluster-glass scenario might be more appropriate. Further studies are in progress in order to clarify an interpretation on this aspect.

4. Conclusion

In the present work, we were interested in understanding how variations of magnetic properties are related to both chemical composition and structural variations of a series of $La_{1-x}MnO_{3\pm\delta}$ manganite phases. We were motivated by the apparent contradictions in published results on such compounds. We thus synthesized eight samples of different La/Mn ratios varying from 0.66 up to 1.02. Let us emphasize that large amounts of powder samples could easily be prepared at low temperature thanks to the use of an original sol–gel method. Accurate determinations of both chemical composition and structure of these samples were obtained by combining several techniques of characterization, so that correlations could be established with the observed magnetic properties. We have shown in particular that through a phase equilibrium, a manganite phase $La_{0.89}MnO_3$ with a high Curie temperature of 295 K is always obtained in a quite large range of initial La/Mn ratio values. This definitely demonstrates that the solubility limit of vacancies on La-site is around 10% in bulk materials, in opposite to previous old or more recent articles [11,13,31]. Thus, besides fundamental aspects, such a result could be interesting for applications requiring the fabrication of manganite compounds with a well-defined Curie temperature. Besides, magnetizations were shown to be influenced by different structural features as parasitic phases, grain boundaries or manganese vacancies. Some unsaturated magnetizations of sample were for instance explained by introducing a non-collinear magnetic behavior of grain boundaries. Finally, as changes of the Curie temperature were observed for samples with a $La/Mn > 0.9$, we showed that a presence of vacancies of Mn sites, whose concentration was evaluated by combined composition/Rietveld refinements, leads to a destruction of long-range ferromagnetic order.

References

[1] J.A.M. Van Roosmalen, E.H.P. Cordfunke, R.B. Helmholdt, H.W. Zandbergen, J. Solid State Chem. 110 (1994) 100–105.
[2] M. Hervieu, R. Mahesh, N. Rangavittal, C.N.R. Rao, Eur. J. Solid State Inorg. Chem. 32 (1995) 79–94.
[3] F. Prado, R.D. Sanchez, A. Caneiro, M.T. Causa, M. Tovar, J. Solid State Chem. 146 (1999) 418–427.
[4] J.A. Alonso, M.J. Martinez-Lope, M.T. Casais, A. Munoz, Solid State Commun. 102 (1) (1997) 7–12.
[5] B.C. Tofield, W.R. Scott, J. Solid State Chem. 10 (1974) 183–194.
[6] J. Töpfer, J.B. Goodenough, J. Solid State Chem. 130 (1997) 117–128.
[7] I. Maurin, P. Barboux, Y. Lassailly, J.-P. Boilot, F. Villain, J. Magn. Magn. Mater. 211 (2000) 139–144.
[8] J.F. Mitchell, D.N. Argyriou, C.D. Potter, D.G. Hinks, J.D. Joergensen, S.D. Bader, Phys. Rev. B 54 (9) (1996) 6172–6182.
[9] R.A. De Souza, M.S. Islam, E. Ivers-Tiffée, J. Mater. Chem. 9 (1999) 1621–1627.
[10] B.C. Hauback, H. Fjellvaeg, N. Sakai, J. Solid State Chem. 124 (1996) 43–51.
[11] V. Ferris, L. Brohan, M. Ganne, M. Tournoux, Eur. J. Solid State Inorg. Chem. 32 (1995) 131–144.
[12] J. Töpfer, J.B. Goodenough, Chem. Mater. 9 (1997) 1467–1474.
[13] A. Arulraj, R. Mahesh, G.N. Subbanna, R. Mahendiran, A.K. Raychaudhuri, C.N.R. Rao, J. Solid State Chem. 127 (1996) 87–91.
[14] J.A.M. Van Roosmalen, H.W. Zandbergen, E.H.P. Cordfunke, W.L. Ijdo, D.J.W. Ijdo, J. Solid State Chem. 114 (1995) 516–523.
[15] A. Sin, P. Odier, Adv. Mater. 12 (9) (2000) 649–652.
[16] A. Sin, J.J. Picciolo, R.H. Lee, F. Gutierrez-Mora, K. Goretta, J. Mat. Sci. Lett. 20 (2001) 1639.
[17] G. Dezanneau, A. Sin, H. Roussel, H. Vincent, M. Audier, Solid State Commun. 121 (2002) 133.
[18] I.G. Krogh Andersen, E. Krogh Andersen, P. Norby, E. Skou, J. Solid State Chem. 113 (1994) 320.
[19] J. Rodriguez-Carvajal, Powder diffraction Abstracts of the Satellite meeting of the XV congress of the International Union of Crystallography, Toulouse 16-19 (1990) 127.
[20] H.M. Rietveld, Powder diffraction 2 (1969) 65.
[21] O.Y. Gorbenko, I.E. Graboy, A.R. Kaul, H.W. Zandbergen, J. Magn. Magn. Mater. 211 (2000) 97.
[22] P.G. Radaelli, M. Marezio, H.Y. Hwang, S.W. Cheong, J. Solid State Chem. 122 (1996) 444.
[23] Q. Huang, A. Santoro, J.W. Lynn, R.W. Erwin, J.A. Borchers, J.L. Peng, R.L. Green, Phys. Rev. B 55 (1997) 14987.
[24] D. Jarosch, Mineral. Petrol. 37 (1987) 15.
[25] S. Bernal, J.A. Diaz, R. Gracia, J.M. Rodriguez-Isquierdo, J. Mater. Sci. 20 (1985) 537.
[26] M.P. Rosynek, D.T. Magnuson, J. Catal. 48 (1977) 417.
[27] Ll. Balcells, B. Martinez, F. Sandiumenge, J. Fontcuberta, J. Magn. Magn. Mater. 211 (2000) 193.
[28] R. Ramesh, R. Mahendiran, A.K. Raychaudhuri, C.N.R. Rao, Appl. Phys. Lett. 68 (1996) 2291.
[29] C. Ritter, M.R. Ibarra, J.M. De Teresa, P.A. Algarabel, C. Marquina, J. Blasco, J. Garcia, S. Oseroff, C.-W. Cheong, Phys. Rev. B 56 (14) (1997) 8902.
[30] L. Sundheendra, A.R. Raju, C.N.R. Rao, Int. J. Inorg. Chem. 2 (2000) 657.
[31] B.V. Slobodin, L.L. Surat, E.V. Vladimirova, J. Alloys Compds. 335 (2002) 115.